Title: Single-cell analysis of prenatal and postnatal human cortical development

One Sentence Summary: Single-cell transcriptomic atlas of human cortical development identifies lineage and sex-specific programs and their implication in brain disorders.

Authors: Dmitry Velmeshev*[#1,2,3], Yonatan Perez*[1,2], Zihan Yan[3], Jonathan E. Valencia[4], David R. Castaneda-Castellanos[5], Li Wang[1,2], Lucas Schirmer[6,7,8], Simone Mayer[1,2,9], Brittney Wick[10], Shaohui Wang[1,2], Tomasz Jan Nowakowski[11], Mercedes Paredes[2], Eric J Huang[1,12], Arnold R Kriegstein[1,2#]

Affiliations: *[1]Eli and Edythe Broad Center of Regeneration Medicine and Stem Cell Research, University of California, San Francisco, CA 94143; [2]Department of Neurology, University of California, San Francisco, CA 94143, [3]Department of Neurobiology, Duke University School of Medicine, Durham, NC 27710; [4]Curio Bioscience, 4030 Fabian Way, Palo Alto, CA 94303, [5]Vizgen Inc. 61 Moulton Street Cambridge, MA 02138, [6]Division of Neuroimmunology, Department of Neurology, Medical Faculty Mannheim, Heidelberg University, Mannheim, Germany, 68167; [7]Mannheim Center for Translational Neuroscience and Institute for Innate Immunoscience, Medical Faculty Mannheim, Heidelberg University, Mannheim, Germany, 68167; [8]Interdisciplinary Center for Neurosciences, Heidelberg University, Heidelberg, Germany, 68167; [9]Hertie Institute for Clinical Brain Research, University of Tübingen, Tübingen, Germany 72076; [10]UC Santa Cruz Genomics Institute, Santa Cruz, CA 95060, [11]Department of Neurological Surgery, University of California, San Francisco, CA 94143; [12]Department of Pathology, University of California, San Francisco, CA 94115.*

[#]Correspondence: arnold.kriegstein@ucsf.edu and dmitry.velmeshev@duke.edu

*These authors contributed equally to this work.

Abstract:

We analyze more than 700,000 single-nucleus RNA-seq profiles from 106 donors during prenatal and postnatal developmental stages and identify lineage-specific programs that underlie the development of specific subtypes of excitatory cortical neurons, interneurons, glial cell types and brain vasculature. By leveraging single-nucleus chromatin accessibility data, we delineate enhancer-gene regulatory networks and transcription factors that control commitment of specific cortical lineages. By intersecting our results with genetic risk factors for human brain diseases, we identify the cortical cell types and lineages most vulnerable to genetic insults of different brain disorders, especially autism. We find that lineage-specific gene expression programs upregulated in female cells are especially enriched for the genetic risk factors of autism. Our study captures the molecular progression of cortical lineages across human development.

Main text

Development of the human cerebral cortex spans months during prenatal stages and years after birth, generating tens to hundreds of cell types across multiple cortical areas. This complex process is orchestrated by lineage-specific gene expression programs that guide the production, migration, differentiation and maturation of neuronal and glial cell types, as well as the formation of projections and neuronal circuits. Alterations in these regulatory gene programs during development lead to the pathogenesis of neurodevelopmental and psychiatric disorders, including autism spectrum disorder (ASD) and schizophrenia (SCZ). Most previous studies have focused on investigating the molecular processes that underly human cortical development

during the second trimester of gestation (*1-5*), the peak of cortical neurogenesis and neuronal migration. These studies have revealed molecular signatures of progenitor cells and neuronal and glial cell types, as well as the early specification of neurons into broad subtypes and their arealization across the cortex. However, later stages of human cortical development, including the third trimester of gestation, birth, and neonatal and early postnatal development, have been largely studied using bulk genomic approaches.

Single-nucleus RNA sequencing analysis of prenatal and postnatal human cortical development

To gain a comprehensive view of human cortical development across prenatal and postnatal stages, we utilized single-nucleus RNA sequencing (snRNA-seq) (*6*) to profile 413,682 nuclei from 108 tissue samples derived from 60 neurotypical individuals. We sampled nuclei from ages spanning from the second trimester of gestation to adulthood, including samples from the third trimester and early postnatal stages that are often excluded or underrepresented in genomic studies of the human brain. We acquired data from the ganglionic eminences, the major source of cortical interneurons (*7, 8*), as well as from the cortex. We used Seurat (*9*) to perform unbiased clustering and UMAP embedding. After removing a cluster of cell debris (**Fig S1A**), we retained 358,663 nuclei. To extend our analyses to more brain samples and nuclei, we integrated our data with published datasets of prenatal and postnatal human cortical development (*10-12*). After data integration (**Fig S1B**), our final dataset included 709,372 nuclei and 169 brain tissue samples from 106 individuals (**Fig 1A**, **Table S1**). We identified clusters corresponding to neural progenitors, as well as the major subtypes of excitatory and inhibitory neurons, glia, and vascular cells (**Fig 1B-C**), indicating that we were able to capture transcriptomic changes underlying differentiation and maturation of cortical cell types across development. We detected similar numbers of genes, transcripts, and mitochondrial RNA ratios across different samples (**Fig S1C**) with a median of 1106 genes and 1609 transcripts per nucleus and some variability sample-to-sample. These relative numbers are comparable with published single-cell genomics data collected from the human brain (*13*), with mature neuron cell types expressing higher numbers of genes and transcripts than other cell types (**Fig S1D**). We did not observe batch effects, with nuclei from different samples well intermixed, and no clusters composed of nuclei from a single sample (**Fig S1E**). Nuclei were captured from the prefrontal, cingulate, temporal, insular and motor cortices (**Fig S1F**). For prenatal samples that were not sex-identified, we determined their sex using sex-specific gene expression (**Fig S1G**). Our dataset included 45 female and 61 male subjects. We observed that nuclei clustered according to developmental age (**Fig 1D**), suggesting that transcriptomic changes associated with development are a major driver of cell identity.

Analysis of specific excitatory neuron and interneuron lineages

We next examined the developmental trajectories of excitatory and inhibitory neurons. First, we selected clusters corresponding to dorsal forebrain progenitors (including radial glia and intermediate precursor cells) as well as clusters containing excitatory neurons. By re-clustering this data and referencing molecularly defined cell types annotated in the Allen Brain Atlas (*14*), we identified clusters corresponding to known subtypes of excitatory neurons, including upper (L2-3) and deep-layer intertelencephalic (L5-6-IT) projection neurons, layer 4 neurons (L4), layer 5 (L5) and layer 6 (L6) corticofugal projection neurons, as well as subplate neurons (SP) that were present transiently during the second trimester (**Fig 2A, Fig S2A**). We next used monocle 3 (*15*),

as well as custom scripts (see **Methods**) to construct cellular trajectories based on snRNA-seq data (**Fig 2A; Fig S2B**), select trajectory branches corresponding to specific lineages, and calculate pseudotime for each nucleus. Pseudotime corresponded well to the developmental age of nuclei in each lineage (**Fig 2A**). We identified several branching points in the trajectory: between two major groups of excitatory neurons: L2-3, L4 and L5-6-IT (Ex1) and L5 and L6 (Ex2), as well as between L4 and L2-3/L5-6-IT (Ex3). Next, we aimed to investigate developmental gene expression changes during differentiation and maturation of GABAergic interneuron (IN) lineages. We selected nuclei from ventral forebrain progenitors, as well as cortical interneurons, re-clustered the data and identified known classes of cortical interneurons (**Fig 2B, Fig S2C**), including interneurons expressing VIP, calretinin (CALB2), reelin (RELN), and nitric acid synthase (NOS), and chandelier (PV-CH) and basket (PV-BSK) interneurons expressing parvalbumin, *MME* and *TAC1*, as well as interneurons expressing somatostatin (SST) and co-expressing *SST* and reelin (SST-RELN). We then reconstructed lineage trajectories corresponding to each interneuron subtype (**Fig 2B, Fig S2D**), as well as point of trajectory divergence, such as trajectory branches including MGE- (IN1) and CGE-derived (IN2) interneurons. We calculated pseudotime for each nucleus, which correlated well with the developmental age of the interneurons. Next, we asked whether different neuronal lineages in the human cortex mature at different rates. We correlated pseudotime with the developmental age in each neuronal lineage and observed that neuronal types fell into two main groups: those that mostly matured by the end of the second trimester, and those whose transcriptome profiles continued to change through the third trimester and after birth (**Fig 2C**). The first group included L5, L5-6-IT and all interneuron subtypes, whereas the second group contained L2-3, L4 and L6 excitatory neurons. This result suggests that certain types of human cortical neurons have a protracted maturation timeline.

Once we isolated trajectory branches corresponding to each neuronal lineage, we sought to identify lineage-specific gene expression programs. We employed an approach that allows identification of lineage-specific programs by comparing dynamic expression profiles of each gene in a lineage of interest to all other neuronal, glial and non-neural lineages (see **Methods**). In addition, we applied this approach to identify genes specific to related lineages in the excitatory neuron and interneuron trajectory branches. In total, we identified 1062 lineage-specific genes and 405 branch-specific genes (**Table S2**). We classified these genes based on the age of onset of gene enrichment (50% of the maximum expression) and performed gene ontology analysis for the genes upregulated at each developmental timepoint (**Fig. 2D**). During the second trimester of gestation, we saw enrichment in pathways related to neurogenesis, differentiation, and process growth. Upregulation of synaptogenesis and ion transport pathways could be observed during the third trimester but was most profound between birth and one year of age. Enrichment in synaptic pathways could be observed until adulthood.

In addition to classifying genes based on their age of appearance, we also characterized dynamic expression patterns of lineage-specific genes. The two most common patterns we observed were transient expression and burst expression where upregulation would start at a certain age and continue into adulthood (**Fig 2E**). Our analysis identified several putative regulators of neuronal lineage commitment, such as transcriptional regulator *MN1* specific to L2-3, L5-6-IT and L4 neurons, noncoding RNAs *CYP1B1-AS1* and *LINC00507* enriched in L2-3 neurons, and *HS3ST4* specific to L5 neurons. We saw that genes enriched in more broad lineage branches tended to be

127 transiently expressed genes, whereas genes specific to mature neuronal cell types mostly
128 followed burst expression patterns (**Fig 2F**). This suggests gradual commitment and specification
129 of neuronal cell types through a series of transient and burst transcriptional events. We also
130 classified additional less common expression patterns, such as biphasic expression (**Fig S2e**) and
131 identified different biological processes enriched for genes with burst and transient expression
132 patterns (**Fig S2F**). Finally, we identified genes dynamically expressed during the specification of
133 subplate neurons by comparing lineages during the second and third trimester of gestation when
134 these cells are present (**Fig S2G**). Using spatial transcriptomic analysis of 140 genes across three
135 developmental timepoints, we were able to identify and visualize the spatial location of cell-
136 specific clusters overlaid on the tissue cytoarchitecture. Focusing on early-emerging lineage-
137 specific genes, we validated the spatiotemporal expression of excitatory layer-specific markers
138 **(Fig 2G-H, Fig S3)**. We observed that broad classes of excitatory neurons in the Ex1, Ex2 and Ex3
139 trajectory branches are restricted to specific cortical layers during the second trimester of
140 gestation. Moreover, several markers of L4 neurons, such as *HPCA* and *GREM2*, are expressed in
141 a layer-restricted manner during the second trimester of gestation suggesting that L4 neuronal
142 identity starts to be specified early in development. The layer identity of most excitatory neurons
143 emerges by birth (**Fig S3**) based on the lineage-specific signatures that we find specify human
144 cortical neurons and their segregation to cortical layers.

145 **Dissection of glial and non-neural lineages**

146 We further focused on the analysis of glial lineages, including astrocytes and oligodendrocytes.
147 We re-clustered glial progenitors, oligodendrocyte precursor cells (OPCs), oligodendrocytes, and
148 astrocytes and performed trajectory analysis (**Fig 3A**). We identified two types of astrocytes:
149 fibrous astrocytes with high expression of *GFAP*, and protoplasmic astrocytes with low expression
150 of *GFAP* and high expression of glutamate transporter GLAST (*SLA1A3*) (**Fig S4A**). Next, we
151 performed identification of lineage-specific genes in the manner described for neuronal lineages
152 (**Table S2**). We first focused on genes that were expressed at the divergence of astrocyte and
153 oligo trajectory branches (**Fig 3B**). We observed well-known transcription factors guiding
154 commitment to the oligo and astrocyte lineages, including *OLIG1*, *OLIG2*, *ID4* and *SOX9*, as well
155 as other putative regulators, such as the zinc finger protein ZCCHC24 specific to the oligo lineage
156 and a DNA binding protein STOX1 enriched in astrocytes. When comparing fibrous and
157 protoplasmic astrocytes, we identified gene programs specific to these cell types (**Fig 3C**). Genes
158 upregulated in protoplasmic astrocytes after birth and during the first year of life were mostly
159 associated with the transport of glutamate and its metabolites, suggesting a maturation program
160 to support neuronal firing during the early postnatal period. For oligodendrocytes we observed
161 that genes upregulated during the second and third trimesters were associated with glial cell
162 differentiation, whereas myelination genes were upregulated after birth and continued to be
163 expressed into adulthood (**Fig 3E**). Analysis of microglia development (**Fig 3F**) identified three cell
164 trajectories (MG-1-3), one of which (MG-3) was associated with highly activated microglia and
165 was present in a small number of samples. These trajectories were confirmed by an alternative
166 analysis using Slingshot (**Fig S4B**) (*16*). We focused on the non-activated microglia trajectories
167 (MG-1 and MG-2) which were differentiated from each other by expression of a pro-
168 inflammatory microglia marker, *IKZF1,* expressed in MG-2. *IKZF1* was the only gene
169 differentiating MG-1 and MG-2, suggesting that these trajectories may represent two different

170 states of the same microglia cell type rather than different subtypes; therefore, we focused on
171 genes developmentally expressed in both of these microglia cell clusters. By performing Gene
172 Ontology (GO) analysis of microglia-specific genes upregulated at different developmental
173 stages, we observed complement genes associated with synaptic pruning upregulated in
174 microglia after birth and during the first year of life (**Fig S4C**, **Fig 3G**). These findings suggest that
175 the developmental period between birth and one year of life is a critical period of synaptic
176 formation and plasticity that involves not only neuronal lineages, but also protoplasmic
177 astrocytes and microglia. Finally, we identified gene programs associated with the maturation of
178 brain endothelial cells and pericytes (**Fig S4D-F**). Our data suggests a coordinated maturation of
179 neuronal and glial cell functions that insures proper formation and maintenance of neuronal
180 circuits.

181 **Integration of with single-cell open chromatin data and identification of lineage-specific gene**
182 **regulatory networks**

183 Epigenetic regulation plays a crucial role in cortical neuron lineage commitment and
184 specification. In order to identify lineage-specific transcriptional and epigenetic regulators of the
185 cortical lineages identified in the snRNA-seq data, we leveraged recently published single-nucleus
186 ATAC-seq (snATAC-seq) data from the developing human cortex during prenatal and postnatal
187 stages (*10, 11, 17, 18*). First, we combined snATAC-seq data from four datasets, obtaining
188 290,239 snATAC-seq profiles from 57 tissue sample and 42 individuals across the second
189 trimester, early postnatal stages of development, as well as adult life. We then utilized Seurat to
190 integrate the resulting snATAC-seq data with our snRNA-seq data and mapped the integrated
191 snATAC-seq data to the snRNA-seq clusters, UMAP space, and cell types (**Fig 4A, see Methods**).
192 We observed that the developmental ages for the snATAC-seq and snRNA-seq profiles are well
193 aligned (**Fig 4A, Fig 1D**). Gene activity (open chromatin in the promoter and gene body) of cell
194 type marker genes suggested that snATAC-seq profiles mapped to corresponding
195 transcriptionally defined neuronal and glial cell types (**Fig S5A**). Next, we repeated the integration
196 and mapping procedure for three major lineage classes: excitatory neurons, interneurons, and
197 glia (astrocytes and oligodendrocytes) (**Fig 4B-D, Fig S5B-D**). We omitted microglia and vascular
198 cells due to a low number of snATAC-seq profiles in these lineages. After mapping snATAC-seq
199 data to the transcriptionally defined lineages, we selected snATAC-seq cells along each lineage
200 branch (**Fig S5B-D)**. Not all lineages could be reliably recovered due to the smaller size of the
201 snATAC-seq dataset and the lack of key developmental stages, such as the third trimester. We
202 therefore focused on lineages that had ATAC cells along the entire span of the trajectory,
203 including four excitatory neuron lineages, five interneuron lineages, and both types of astrocytes
204 and oligodendrocytes as indicated in **Fig 4B-D**. Plots of lineage-specific gene activity over
205 pseudotime demonstrated that we accurately mapped and selected lineage-specific snATAC-seq
206 profiles (**Fig 4B-D)**. Finally, we leveraged SCENIC+ (*19*), a recently developed algorithm that uses
207 paired single-cell transcriptomic and open chromatin data to identify enhancer gene regulatory
208 networks (eGRN) and candidate transcription factors that regulate expression of target genes in
209 these networks. We applied SCENIC+ to the snRNA-seq and snATAC-seq profiles in each lineage
210 to identify open chromatin regions correlated with pseudotime, putative enhancers, candidate
211 transcription factors (TF) that bind them, and their association with lineage-specific dynamically
212 expressed genes (**Table S3**). In total, we identified 42 transcription factors regulating 1373

213 lineage-specific genes through predicted binding of 4846 regulatory chromatin regions. We
214 observed networks regulated by previously known lineage-specific transcriptional regulators,
215 such as SOX5 in deep-layer projection neurons (**Fig 4B**), LHX6 in MGE-derived PV and SST
216 interneurons (**Fig 4C, Table S3**), OLIG2 in oligodendrocytes and SOX9 in astrocytes (**Fig 4D**).
217 Additionally, we identified previously unrecognized (at the best of our knowledge) putative
218 lineage-specific transcriptional regulators, such as BACH2, predicted to regulate several key
219 deep-layer transcription factors in L5 neurons, including FOXP2 and FEZF2, as well as NFIX and
220 ZNF184 specific to L2-3 neurons and regulating expression of the upper-layer master
221 transcription factor, CUX2 (**Fig 4B**). Our results also suggest the role of the transcription factor
222 MAFB in parvalbumin interneuron specification (**Fig 4C**), as well as of FOXN2 and RFX4 in
223 determining the fate of oligodendrocytes and protoplasmic astrocytes, respectively (**Fig 4D**). Our
224 data sheds new light on epigenetic control of neural lineage commitment and identifies putative
225 transcription factors and regulatory networks that define the fate of specific human cortical
226 neuronal and glial cell types.

227 **Identification of region and sex-enriched lineage-specific gene programs**

228 Since we sampled our transcriptomic data from different cortical regions, we asked whether
229 lineage-specific developmental gene expression profiles might be spatially defined, and vary
230 depending on cortical area. We focused on the frontal/prefrontal cortex (PFC) since we had the
231 most complete sampling of this cortical area across developmental stages (**Fig S6A**). We
232 compared each neuronal and glial lineage trajectory in the PFC to the trajectories in all other
233 cortical areas and identified PFC-enriched developmentally regulated genes in each lineage
234 (**Table S4**). We observed more PFC-specific genes in excitatory neuron lineages, especially in
235 intertelencephalic upper (L2-3) and deep-layer (L5-6-IT) neurons, as well as in astrocytes and
236 oligodendrocytes, whereas most interneuron lineages and microglia expressed fewer PFC-
237 specific genes (**Fig S6B**). After performing GO analysis for PFC genes specific to neuronal lineages,
238 we observed enrichment in cell adhesion and synaptic transmission pathways (**Fig S6C**). Analysis
239 of glia-specific PFC genes demonstrated enrichment in different categories of biological pathways
240 associated with cell division and cell migration (**Fig S6D**). Examples of neuronal PFC genes
241 included synaptojanin 2 binding protein *SYNJ2BP* regulating receptor localization and signal
242 transduction at the synapse and the cation channel *TRPC7* (**Fig S6E**). PFC fibrous astrocytes
243 upregulated R-spondin 2 (*RSPO2*) and Frizzled Class Receptor 8 (*FZD8*), which both participate in
244 Wnt signaling and cell migration. Our results suggest cortical areal differences in lineage-specific
245 transcriptomic programs, with synaptic genes upregulated in neuronal cell types and cell division
246 and cell migration programs activated in glial cells in the developing PFC. PFC-specific expression
247 of synaptic genes in neuronal cell types suggests regional specification of neuronal circuits during
248 development.

249 We next asked whether the development of specific cellular lineages is modulated in a sex-
250 dependent manner. For each lineage analyzed, we isolated female and male nuclei (**Fig 5A**, **Fig**
251 **S7A**) and identified dynamically expressed genes enriched during either female or male
252 development. In total, we identified 740 female-enriched genes and 312 male-enriched genes
253 (**Table S5**). Only a small fraction of male genes showed female/male enrichment in a lineage-
254 specific manner (20/312, 6.4%), whereas more than half of female genes showed lineage
255 specificity of sex enrichment (510/740, 69%). Despite several top female-enriched genes located

256 on X and Y chromosomes (including *XIST* and *PCDH11Y*), sex-enriched genes were evenly
257 distributed across all chromosomes (**Fig S7B**), suggesting that sex-dependent developmental
258 modulation of gene expression is not directly dependent on transcription from the sex
259 chromosomes. We next performed GO analysis of female and male-enriched genes, focusing on
260 the neuronal, astrocyte and oligodendrocyte lineages where we had large number of samples
261 and nuclei from both sexes. We observed substantial difference between the biological processes
262 associated with female and male-enriched genes: female genes were involved in developmental
263 processes, including cell adhesion, CNS development, synaptic transmission and membrane
264 potential regulation (**Fig. 5B**), whereas male genes were associated with RNA metabolism and
265 translation (**Fig. 5C**). Only a small number of male-specific genes such as *YBX1* and *LINGO1* were
266 associated with developmental processes; however, these genes were enriched across multiple
267 male lineages (**Fig S7C**). We classified sex-enriched genes according to their dynamic expression
268 pattern and saw that the majority were expressed transiently (**Fig. 5D)**, with over 90% having
269 peak expression during the second trimester (**Table S5**). This suggest early and transient sex-
270 dependent developmental modulation of cortical lineages. Sex-enriched genes were more
271 abundant in excitatory neuron lineages compared to interneurons (**Fig 5E**) and were also
272 abundant in female fibrous astrocytes. Several top lineage-specific female-enriched genes were
273 associated with neuronal, glial and endothelial development (**Fig 5F, Fig S7D**). These included
274 nuclear hormone receptor/transcription factor *RORA* in L2-3 neurons, synaptic protein
275 neurexophilin 3 (*NXPH3*) in L6 neurons, transcription factor *HES4* in fibrous astrocytes, and an
276 actin filament depolymerization enzyme, *MICAL3,* in oligodendrocytes. Overall, our results point
277 to modulation of neuronal and glial developmental programs during second trimester female
278 brain development.

279 **Enrichment of lineage-specific developmental gene programs for risk factors of brain disorders**

280 Once we defined lineage and sex-specific developmental gene programs in human cortical cell
281 types, we sought to investigate how these transcriptional programs may be affected in
282 neurodevelopmental, psychiatric, and neurodegenerative disorders. We compiled all lineage-
283 specific gene signatures for excitatory neurons, astrocytes, oligodendrocytes, interneurons,
284 microglia, endothelial cells and pericytes, in total obtaining 2796 unique genes, and divided them
285 into 5 groups based on their age of expression onset (50% of max expression). We then
286 overlapped this gene list with lists of rare gene variants associated with the risk of ASD from the
287 Simons Foundation Autism Research Initiative (SFARI) Gene database (*20*), as well as GWAS genes
288 for the risk of SCZ (*21*), bipolar disorder (BPD) (*22*) and Alzheimer's disease (AD) (*23*) (**Fig 6A,**
289 **Table S6**). We observed a large enrichment for genes associated with risk for ASD, SCZ and BPD
290 in the second trimester, with expression of ASD and BPD risk genes extending to the third
291 trimester. The risk of neurodevelopmental disorders dropped during later stages of
292 development. Expression of ASD risk genes remained mostly flat and only slightly above the
293 significance level, demonstrating a pattern different from neurodevelopmental and psychiatric
294 disorders. We next analyzed enrichment of disease risk genes across cortical lineages (**Fig 6B**).
295 We were able to detect significant enrichment for ASD risk genes in L5-6-IT and L5 neurons,
296 whereas AD risk genes were enriched in microglia. We focused on ASD since we observed the
297 strongest enrichment for the risk of this disorder among developmentally regulated genes, and
298 because a large amount of genetic risk data is available for this disorder. We observed

299 developmental enrichment of ASD risk genes with SFARI score 2 and 3 but not score 1 and did
300 not find enrichment in syndromic ASD genes (**Fig 6C**). We observed a significant enrichment
301 among high-confidence ASD risk genes (ASD-HC) based on the TADA analysis (*24*). We conclude
302 that the genetic burden of ASD has the potential to affect the development of specific neuronal
303 cell types, especially deep-layer intertelencephalic projection neurons and L5 neurons. We next
304 explored enrichment of ASD risk genes in sex-specific developmental programs. We observed
305 strong enrichment of female-specific developmental genes in both SFARI and HC-ASD gene lists
306 (**Fig 6D**). Male-specific genes were less frequently found among SFARI genes, and we did not find
307 a meaningful overlap between male-enriched and high-confidence ASD genes. This finding points
308 to a strong enrichment of the genetic risk of ASD among developmental genes that are more
309 highly expressed in female cells. SFARI genes were enriched in female cells across multiple
310 neuronal cell types, especially the subplate and L6 excitatory neurons, as well as
311 oligodendrocytes and fibrous astrocytes, but not in microglia or vascular cell types (**Fig 6E**). This
312 suggests a role of the subplate in the pathogenesis of ASD. Examples of female-specific high-
313 confidence ASD risks genes included the subplate-specific transcription factor *NR4A2* and the
314 neuronal transcription factor *MEF2C* that were upregulated in female subplate cells, as well as a
315 regulator of axon guidance and synaptogenesis, neurexin 2 (*NRXN2),* and *PCDH15* encoding a cell
316 adhesion molecule in female L6 neurons (**Fig 6G**). Our findings provide strong evidence
317 supporting the ASD female protective effect hypothesis (*25*), and suggest that fine-tuning of
318 cortical cell lineages by sex-specific developmental programs can contribute to the male bias in
319 the pathogenesis of ASD.

320 **Discussion**

321 By generating single-nucleus RNA-seq data from the developing human cortex and integrating
322 the findings with previously published datasets, we performed a large-scale unbiased
323 transcriptomic analysis of human cortical development throughout the lifespan. By
324 reconstructing single-cell trajectories and identifying genes that are expressed in a lineage-
325 specific manner we created a compendium of developmental programs for all the major cortical
326 cell types. By integrating our data with published single-cell chromatin accessibility datasets, we
327 identified enhancer-gene regulatory networks and transcription factors that are predicted to
328 control the commitment and differentiation of specific cortical neural lineages. In addition, we
329 characterized sex and brain region-specific gene programs that are used by specific lineages of
330 cortical cell types. We find that female-enriched genes are associated with neurodevelopmental
331 processes, whereas male-enriched genes are involved in protein translation control, suggesting
332 sex-specific variation of developmental trajectories. We also find that developmental gene
333 programs utilized by cortical excitatory neurons, astrocytes and oligodendrocytes are the most
334 region-specific. Interneurons, in contrast, express few region-specific genes during development,
335 consistent with data on regional signatures of cortical cell types in the mature human brain (*26*).

336 We investigated the enrichment of genetic risk factors for brain disorders, focusing on ASD, and
337 found that the developmental programs of both deep-layer intratelencephalic and corticofugal
338 projection neurons are enriched for ASD risk genes. These data are in agreement with previous
339 reports of enrichment of ASD genes in deep-layer cortical neurons during mid-gestation (*27, 28*)
340 but also suggest that both deep-layer neurons projecting to other cortical areas and to subcortical
341 locations could be affected. We previously reported that upper-layer cortical excitatory neurons

342 are most dysregulated in the cortex of idiopathic ASD patients (*29*). It would be an important
343 future direction to elucidate how changes in pan-excitatory neuron programs during
344 development can culminate in dysfunction of specific cortical neuronal populations, such as L2-3
345 neurons. It would also be valuable to explore whether the molecular pathology of upper-layer
346 neurons is specific to idiopathic ASD, and whether it is driven by common gene variants, rather
347 than rare variants with strong effect sizes (*30*). In addition, we observed a strong enrichment of
348 ASD genetic risk factors among female-specific developmental genes. Since these female-
349 enriched ASD risk genes have higher expression in females during cortical development, is
350 possible that this higher baseline expression renders female brain more resistant to genetic
351 insults causing autism, especially to haploinsufficiency that can reduce transcript or protein
352 expression by affecting one of the two alleles. This finding might explain the 4:1 male to female
353 ratio of individuals affected by ASD and suggests the importance of sexual dimorphism in human
354 brain development. However, the role of sex hormones in the increased male to female ratio in
355 ASD is not to be discounted, and additional studies are needed to reconcile the role of early
356 development and later sex-specific processes in the pathogenesis of autism. Our preliminary
357 findings indicate the cell type-specific risk of BPD and SCZ, but more detailed genetic studies are
358 needed to further dissect cell type and developmental stage vulnerability. The data generated
359 here may help enable fine-grained understanding of human brain development and provide
360 insight into mechanisms of neurodevelopmental disorders.

361 Our study, however, is limited by the technical difficulty of integrating snRNA-seq and scATAC-
362 seq data as well as by the lack of inclusion of earlier developmental stages, such as the first
363 trimester, due to challenges of integrating scRNA-seq and snRNA-seq datasets. Overcoming these
364 obstacles will allow for even more comprehensive future understanding of how specific human
365 cortical lineages develop. Moreover, single-cell epigenetic analyses of human brain development
366 would be necessary to determine whether imprinting plays a role in regulating sex enrichment
367 of developmentally expressed genes.

368 **Materials and methods summary**

369 Brain tissue samples were sectioned using a cryostat to collect coronal cortical sections, lysed
370 and ultracentrifuged to isolate nuclei. Nuclei were captured using 10x Genomics Single Cell 3' v.2
371 kits.
372 Raw sequencing data were processed using 10x Genomics CellRanger and aligning reads to
373 unsliced human transcriptome to capture reads from premRNAs. Dataset integration was
374 performed using Harmony based on 10x chemistry, and clustering and UMAP embedding was
375 carried out with Seurat. Monocle 3 was used to reconstruct lineage trajectories, and custom
376 scripts were used to identify lineage-specific dynamically expressed genes (Supplementary
377 Materials).
378 scATAC-seq data were integrated with snRNA-seq data using canonical correlation analysis in
379 Seurat, after which different scATAC-seq chemistries were integrated using Harmony. Enhancer
380 gene regulatory networks were identified using SCENIC+.
381

Figure 1. Brain tissue samples used for data collection and initial clustering of snRNA-seq data. A) Overview of the tissue samples used in the current study, including the number of individuals, as well as ages and brain regions captured in the snRNA-seq dataset. MGE-medial ganglionic eminence, LGE-lateral ganglionic eminence, CGE-caudal ganglionic eminence, GE- ganglionic eminence. **B)** Clustering of the entire dataset, with the major lineages labeled. **C)** Expression of cell type-specific markers used to determine cardinal lineages. **D)** Nuclei labeled by their developmental age.

Figure 2. Analysis of excitatory and inhibitory neuron lineages. A) Cell types, reconstructed single-cell trajectories, and age distribution for subtypes of excitatory neurons. L2-3 – upper-layer cortico-cortical projection neurons, L4 – layer 4 neurons, L5-6-IT – deep-layer intratelencephalic projection neurons, L6 – layer 6 neurons, L5 – layer 5 neurons, SP – subplate neurons. **bB**Identification of interneuron trajectories. **C)** Rates of maturation of subtypes of excitatory neurons and interneurons. **D)** Gene ontology analysis of genes with different age of onset of expression. **E)** Examples of top lineage and branch-specific genes with transient and burst expression patterns. **F)** Number of transient and burst genes in specific lineages and branches. **G)** Spatial transcriptomic analysis of 140 lineage-specific genes, showing the spatial map of annotated cell-types across development (GW22 = 22 weeks of gestation; 2wk = 2 weeks postnatal; 25yo = 25-year-old; PFC = prefrontal cortex). **H)** Examples of deep-layer neuronal markers with early patterned layer-specific expression (putative layer location is in brackets).

Figure 3. Analysis of inhibitory cortical interneuron lineages. A) Clusters and trajectories of glial progenitors, astrocytes and oligodendrocytes. **B)** Sample genes specific to oligodendrocyte and astrocyte lineage branches. **C)** Examples of top dynamically expressed genes specific to fibrous and protoplasmic astrocytes. **D)** Gene ontology analysis of protoplasmic astrocyte-specific genes expressed during the first year of life. **E)** Pathways enriched for oligo lineage-specific genes expressed at different developmental stages. **F)** Analysis of microglia lineages. **G)** Temporal patterns of developmental microglia genes.

Figure 4. Identification of lineage-specific epigenetic and transcriptional regulators. A) Integration of snRNA-seq and scATAC-seq data. scATAC-seq data was mapped on the scRNA-seq coordinates, clusters and cell types. **B-D)** Analysis of enhancer gene regulatory networks (eGRNs) in excitatory neuron lineages **(B)**, as well as interneurons **(C)** and glial lineages **(D)**. Network plots (eGNRs) display transcription factors predicted to bind enhancer regions to regulate lineage-specific transcriptional programs. Edge colors indicate regulation by different transcription factors. Top 20 genes based on the predicted confidence of interaction are shown for each transcription factors network.

Figure 5. Analysis of sex-specific developmental programs in human cortex. A) Female and male developmental trajectories of excitatory neurons, interneurons, astrocytes and oligodendrocytes. **B-C)** Gene ontology analysis of female and male-enriched genes. **D)** Dynamic expression patterns of sex-enriched genes. **E)** Sex enrichment of developmental gene expression across neuronal and glial lineages. **F)** Examples of top female-enriched genes in specific lineages.

Fig 6. Lineage enrichment of ASD risk genes. A) Enrichment of disease risk genes across developmental stages. **B)** Disease risk gene enrichment across lineages and lineage branches of neuronal, glial, and vascular cell types. Red squares indicate statistical significance. **C)** Enrichment of lineage-specific developmentally regulated ASD risk genes of different categories and evidence scores. **D)** Overlap between ASD risk genes and female and male-enriched developmental gene programs. **E)** Enrichment of sex-specific genes across specific lineages. **F)** Temporal patterns of female-enriched genes that are known risk factors for ASD.

References and Notes:

1. A. Bhaduri *et al.*, An atlas of cortical arealization identifies dynamic molecular signatures. *Nature* **598**, 200-204 (2021).
2. U. C. Eze, A. Bhaduri, M. Haeussler, T. J. Nowakowski, A. R. Kriegstein, Single-cell atlas of early human brain development highlights heterogeneity of human neuroepithelial cells and early radial glia. *Nature Neuroscience* **24**, 584-594 (2021).
3. T. J. Nowakowski *et al.*, Spatiotemporal gene expression trajectories reveal developmental hierarchies of the human cortex. *Science* **358**, 1318-1323 (2017).
4. R. S. Ziffra *et al.*, Single cell epigenomic atlas of the developing human brain and organoids. *bioRxiv*, 2019.2012.2030.891549 (2020).
5. M. Li *et al.*, Integrative functional genomic analysis of human brain development and neuropsychiatric risks. *Science* **362**, (2018).
6. B. B. Lake *et al.*, Neuronal subtypes and diversity revealed by single-nucleus RNA sequencing of the human brain. *Science* **352**, 1586-1590 (2016).
7. D. V. Hansen *et al.*, Non-epithelial stem cells and cortical interneuron production in the human ganglionic eminences. *Nat Neurosci* **16**, 1576-1587 (2013).
8. T. Ma *et al.*, Subcortical origins of human and monkey neocortical interneurons. *Nat Neurosci* **16**, 1588-1597 (2013).
9. A. Butler, P. Hoffman, P. Smibert, E. Papalexi, R. Satija, Integrating single-cell transcriptomic data across different conditions, technologies, and species. *Nature Biotechnology* **36**, 411-420 (2018).
10. C. A. Herring *et al.*, Human prefrontal cortex gene regulatory dynamics from gestation to adulthood at single-cell resolution. *Cell* **185**, 4428-4447.e4428 (2022).
11. A. E. Trevino *et al.*, Chromatin and gene-regulatory dynamics of the developing human cerebral cortex at single-cell resolution. *Cell* **184**, 5053-5069.e5023 (2021).
12. S. I. Ramos *et al.*, An atlas of late prenatal human neurodevelopment resolved by single-nucleus transcriptomics. *Nature Communications* **13**, 7671 (2022).
13. N. Habib *et al.*, Massively parallel single-nucleus RNA-seq with DroNc-seq. *Nat Methods* **14**, 955-958 (2017).
14. R. D. Hodge *et al.*, Conserved cell types with divergent features in human versus mouse cortex. *Nature* **573**, 61-68 (2019).
15. J. Cao *et al.*, The single-cell transcriptional landscape of mammalian organogenesis. *Nature* **566**, 496-502 (2019).
16. K. Street *et al.*, Slingshot: cell lineage and pseudotime inference for single-cell transcriptomics. *BMC Genomics* **19**, 477 (2018).
17. R. S. Ziffra *et al.*, Single-cell epigenomics reveals mechanisms of human cortical development. *Nature* **598**, 205-213 (2021).
18. S. Domcke *et al.*, A human cell atlas of fetal chromatin accessibility. *Science* **370**, eaba7612 (2020).
19. C. Bravo González-Blas *et al.*, SCENIC+: single-cell multiomic inference of enhancers and gene regulatory networks. *Nature Methods*, (2023).
20. B. S. Abrahams *et al.*, SFARI Gene 2.0: a community-driven knowledgebase for the autism spectrum disorders (ASDs). *Mol Autism* **4**, 36 (2013).

21. Y. Wu, X. Li, J. Liu, X. J. Luo, Y. G. Yao, SZDB2.0: an updated comprehensive resource for schizophrenia research. *Hum Genet* **139**, 1285-1297 (2020).
22. X. Li *et al.*, dbBIP: a comprehensive bipolar disorder database for genetic research. *Database* **2022**, baac049 (2022).
23. C. Bellenguez *et al.*, New insights into the genetic etiology of Alzheimer's disease and related dementias. *Nature Genetics* **54**, 412-436 (2022).
24. F. K. Satterstrom *et al.*, Large-Scale Exome Sequencing Study Implicates Both Developmental and Functional Changes in the Neurobiology of Autism. *Cell* **180**, 568-584.e523 (2020).
25. E. B. Robinson, P. Lichtenstein, H. Anckarsäter, F. Happé, A. Ronald, Examining and interpreting the female protective effect against autistic behavior. *Proceedings of the National Academy of Sciences* **110**, 5258-5262 (2013).
26. B. Tasic *et al.*, Shared and distinct transcriptomic cell types across neocortical areas. *Nature* **563**, 72-78 (2018).
27. N. N. Parikshak *et al.*, Integrative functional genomic analyses implicate specific molecular pathways and circuits in autism. *Cell* **155**, 1008-1021 (2013).
28. A. J. Willsey *et al.*, Coexpression networks implicate human midfetal deep cortical projection neurons in the pathogenesis of autism. *Cell* **155**, 997-1007 (2013).
29. T. Gaugler *et al.*, Most genetic risk for autism resides with common variation. *Nat Genet* **46**, 881-885 (2014).

Acknowledgments: We thank the NIH's Brain Research through Advancing Innovative Neurotechnologies Initiative - Cell Census Network (BICCN) and The Brain Cell Data Center (BCDC) at the Allen Institute for Brain Science, as well as all of its members for the support of this work and helpful discussions.

Funding: This study was funded by U01MH114825 awarded to ARK , 5R35NS097305 awarded to ARK, NINDS P01 NS083513 Neuropathology Core to EJH, Quantitative Biosciences Institute's BOLD & BASIC Fellowship to DV and NIMH K99/R00 Award to DV, New York Stem Cell Foundation Robertson Neuroscience Investigator Award to TJN, Deutsche Forschungsgemeinschaft to SM and NHGRI 2U24HG002371-23 to BW.

Authors contributions: DV designed the project, acquired tissue collection, performed nuclei isolation and 10x Genomics capture, analyzed the data and wrote the manuscript. YP performed spatial transcriptomic experiments, nuclei isolation and 10x Genomics capture and edited the manuscript. ZY helped with the analysis code and performed analysis of the oligodendrocyte lineage. JEV and DRC performed probe design and analysis of spatial transcriptomics data. LW performed spatial transcriptomic experiments. LS acquired adult samples, performed nuclei isolation and 10x Genomics capture. SM performed nuclei isolation and 10x Genomics capture. BW developed Cell Browser visualization tools. SW acquired second trimester tissue samples. TJN performed regional tissue dissections. MP and EJH acquired third trimester and early postnatal samples. ARK designed and supervised the project and edited the manuscript. All authors read the manuscript.

Competing interests: Authors have no competing interests.

Data and materials availability: Raw data can be accessed at the NeMo Archive, accession number nemo:dat-3ah9h9x (https://assets.nemoarchive.org/dat-3ah9h9x). Analyzed data (cell-count matrix and metadata) can be accessed through the UCSC Cell Browser, collection human-cortical-dev (https://pre-postnatal-cortex.cells.ucsc.edu), and at cellxgene (https://cellxgene.cziscience.com/collections/bacccb91-066d-4453-b70e-59de0b4598cd). Code is available at https://github.com/velmeshevlab/dev_hum_cortex and https://doi.org/10.5281/zenodo.7245297.

Supplementary Materials:
Materials and Methods
Table S1 – S6
Fig S1 – S7
References (31 – 37)

1. A. Bhaduri *et al.*, An atlas of cortical arealization identifies dynamic molecular signatures. *Nature* **598**, 200-204 (2021).
2. U. C. Eze, A. Bhaduri, M. Haeussler, T. J. Nowakowski, A. R. Kriegstein, Single-cell atlas of early human brain development highlights heterogeneity of human neuroepithelial cells and early radial glia. *Nature Neuroscience* **24**, 584-594 (2021).
3. T. J. Nowakowski *et al.*, Spatiotemporal gene expression trajectories reveal developmental hierarchies of the human cortex. *Science* **358**, 1318-1323 (2017).
4. R. S. Ziffra *et al.*, Single cell epigenomic atlas of the developing human brain and organoids. *bioRxiv*, 2019.2012.2030.891549 (2020).
5. M. Li *et al.*, Integrative functional genomic analysis of human brain development and neuropsychiatric risks. *Science* **362**, (2018).
6. B. B. Lake *et al.*, Neuronal subtypes and diversity revealed by single-nucleus RNA sequencing of the human brain. *Science* **352**, 1586-1590 (2016).
7. D. V. Hansen *et al.*, Non-epithelial stem cells and cortical interneuron production in the human ganglionic eminences. *Nat Neurosci* **16**, 1576-1587 (2013).
8. T. Ma *et al.*, Subcortical origins of human and monkey neocortical interneurons. *Nat Neurosci* **16**, 1588-1597 (2013).
9. A. Butler, P. Hoffman, P. Smibert, E. Papalexi, R. Satija, Integrating single-cell transcriptomic data across different conditions, technologies, and species. *Nature Biotechnology* **36**, 411-420 (2018).
10. C. A. Herring *et al.*, Human prefrontal cortex gene regulatory dynamics from gestation to adulthood at single-cell resolution. *Cell* **185**, 4428-4447.e4428 (2022).
11. A. E. Trevino *et al.*, Chromatin and gene-regulatory dynamics of the developing human cerebral cortex at single-cell resolution. *Cell* **184**, 5053-5069.e5023 (2021).
12. S. I. Ramos *et al.*, An atlas of late prenatal human neurodevelopment resolved by single-nucleus transcriptomics. *Nature Communications* **13**, 7671 (2022).
13. N. Habib *et al.*, Massively parallel single-nucleus RNA-seq with DroNc-seq. *Nat Methods* **14**, 955-958 (2017).

14. R. D. Hodge *et al.*, Conserved cell types with divergent features in human versus mouse cortex. *Nature* **573**, 61-68 (2019).
15. J. Cao *et al.*, The single-cell transcriptional landscape of mammalian organogenesis. *Nature* **566**, 496-502 (2019).
16. K. Street *et al.*, Slingshot: cell lineage and pseudotime inference for single-cell transcriptomics. *BMC Genomics* **19**, 477 (2018).
17. R. S. Ziffra *et al.*, Single-cell epigenomics reveals mechanisms of human cortical development. *Nature* **598**, 205-213 (2021).
18. S. Domcke *et al.*, A human cell atlas of fetal chromatin accessibility. *Science* **370**, eaba7612 (2020).
19. C. Bravo González-Blas *et al.*, SCENIC+: single-cell multiomic inference of enhancers and gene regulatory networks. *Nature Methods*, (2023).
20. B. S. Abrahams *et al.*, SFARI Gene 2.0: a community-driven knowledgebase for the autism spectrum disorders (ASDs). *Mol Autism* **4**, 36 (2013).
21. Y. Wu, X. Li, J. Liu, X. J. Luo, Y. G. Yao, SZDB2.0: an updated comprehensive resource for schizophrenia research. *Hum Genet* **139**, 1285-1297 (2020).
22. X. Li *et al.*, dbBIP: a comprehensive bipolar disorder database for genetic research. *Database* **2022**, baac049 (2022).
23. C. Bellenguez *et al.*, New insights into the genetic etiology of Alzheimer's disease and related dementias. *Nature Genetics* **54**, 412-436 (2022).
24. F. K. Satterstrom *et al.*, Large-Scale Exome Sequencing Study Implicates Both Developmental and Functional Changes in the Neurobiology of Autism. *Cell* **180**, 568-584.e523 (2020).
25. E. B. Robinson, P. Lichtenstein, H. Anckarsäter, F. Happé, A. Ronald, Examining and interpreting the female protective effect against autistic behavior. *Proceedings of the National Academy of Sciences* **110**, 5258-5262 (2013).
26. B. Tasic *et al.*, Shared and distinct transcriptomic cell types across neocortical areas. *Nature* **563**, 72-78 (2018).
27. N. N. Parikshak *et al.*, Integrative functional genomic analyses implicate specific molecular pathways and circuits in autism. *Cell* **155**, 1008-1021 (2013).
28. A. J. Willsey *et al.*, Coexpression networks implicate human midfetal deep cortical projection neurons in the pathogenesis of autism. *Cell* **155**, 997-1007 (2013).
29. D. Velmeshev *et al.*, Single-cell genomics identifies cell type-specific molecular changes in autism. *Science* **364**, 685-689 (2019).
30. T. Gaugler *et al.*, Most genetic risk for autism resides with common variation. *Nat Genet* **46**, 881-885 (2014).

606 **Supplementary Materials**

607 **Materials and Methods**

608 **Sample acquisition and selection**

609 Samples were acquired from three different sources. 1) De-identified second-trimester tissue
610 samples were collected at the Zuckerberg San Francisco General Hospital with previous patient
611 consent in strict observance of the legal and institutional ethical regulations. Protocols were
612 approved by the Human Gamete, Embryo, and Stem Cell Research Committee (institutional
613 review board) at the University of California, San Francisco. These fresh tissue samples were
614 dissected and snap-frozen in isopentane on dry ice. 2) De-identified second-trimester, third
615 trimester and early postnatal tissue samples were obtained at the UCSF Pediatric
616 Neuropathology Research Laboratory led by Dr. Eric Huang. These samples were acquired with
617 patient consent in strict observance of the legal and institutional ethical regulations and in
618 accordance to research protocols approved by the UCSF IRB committee. These samples were
619 dissected and snap-frozen either on a cold plate placed on a slab of dry ice or in isopentane on
620 dry ice. 3) Banked de-identified second-trimester, third trimester, early postnatal and adult tissue
621 samples were obtained from the University of Maryland Brain and Tissue Bank through the NIH
622 NeuroBioBank.

623 For postnatal ages, samples from individuals with known history of brain disorders or brain
624 trauma were excluded from downstream analyses. For prenatal samples, samples with unusual
625 neuropathology following pathological examination, as well as samples positive for commonly
626 tested chromosomal aberrations, were excluded. Prior to performing nuclei isolation and single-
627 nucleus RNA sequencing, samples were screened for RNA quality by collecting 100um-thick
628 cryosections, isolating total RNA and measuring RNA Integrity Number (RIN) using the Agilent
629 2100 Bioanalyzer instrument. Only samples with RIN >= 6.5 were included in the study.

630 **Nuclei isolation and generation of single-nucleus RNA-seq data using 10x Genomics platform**

631 40 mg of sectioned brain tissue was homogenized in 5 mL of RNAase-free lysis buffer (0.32M
632 sucrose, 5 mM $CaCl^2$, 3 mM $MgAc^2$, 0.1 mM EDTA, 10 mM Tris-HCl, 1 mM DTT, 0.1% Triton X-100
633 in DEPC-treated water) using glass dounce homogenizer (Thomas Scientific, Cat # 3431D76) on
634 ice. The homogenate was loaded into a 30 mL thick polycarbonate ultracentrifuge tube (Beckman
635 Coulter, Cat # 355631). 9 mL of sucrose solution (1.8 M sucrose, 3 mM $MgAc^2$, 1 mM DTT, 10 mM
636 Tris-HCl in DEPC-treated water) was added to the bottom of the tube with the homogenate and
637 centrifuged at 107,000 g for 2.5 hours at 4°C. Supernatant was aspirated, and the nuclei
638 containing pellet was incubated in 250 uL of DEPC-treated water-based PBS for 20 min on ice
639 before resuspending the pellet. The nuclear suspension was filtered twice through a 30 um cell
640 strainer. Nuclei were counted using a hemocytometer and diluted to 2,000 nuclei/uL before
641 performing single-nuclei capture on the 10X Genomics Single-Cell 3' system. Usually, the target
642 capture of 3,000 nuclei per sample was used; the 10x capture and library preparation protocol
643 was used without modification. Single-nucleus libraries from individual samples were pooled and
644 sequenced on the NovaSeq 6000 machine (average depth 60,000 reads/nucleus).

645 **snRNA-seq data processing with 10X Genomics CellRanger software and data filtering**

646 For library demultiplexing, fastq file generation and read alignment and UMI quantification,
647 CellRanger software v 1.3.1 was used. CellRanger was used with default parameters, except for
648 using pre-mRNA reference file (ENSEMBL GRCh38) to insure capturing intronic reads originating
649 from pre-mRNA transcripts abundant in the nuclear fraction.

650 Individual expression matrices containing numbers of Unique molecular identifiers (UMIs) per
651 nucleus per gene were filtered to retain nuclei with at least 400 genes expressed and less than
652 10% of total UMIs originating from mitochondrial and ribosomal RNAs. Individual matrices were
653 combined prior to pre-processing and clustering with Seurat.

654 **snRNA-seq dataset integration, dimensionality reduction, UMAP embedding, clustering and**
655 **cell type identification**

656 All of the following bioinformatics analysis steps are documented in an R script available at
657 https://doi.org/10.5281/zenodo.7245297.

658 In order to integrate snRNA-seq datasets, we utilized Harmony (*31*) integration using the 10x
659 Genomics chemistry version as the grouping variable. Downstream data preprocessing,
660 normalization, variable feature selection and PCA was performed using the standard Seurat
661 pipeline (*32*). Selection of significant principal components was done using the elbow method.
662 The selected components were used to perform UMAP embedding and clustering using the
663 Louvain method. The identity of specific lineages and cell types was determined based on
664 expression of known marker genes, as is shown in Figure 1 and Figure S1.

665 **Sex determination**

666 To determine the sex of individuals for which sex information was not available, we aggregated
667 gene expression of all nuclei by individual and plotted individual-wise expression of the following
668 genes: *XIST*, *DDX3Y*, *KDM5D*, *USP9Y*, *ZFY*, *EIF1AY*, *UTY*.

669 **Trajectory reconstruction and isolation of individual lineages**

670 Seurat UMAP coordinates were imported into monocle3 (*33*) for trajectory reconstruction.
671 learn_graph function with custom graph_control options was used to construct the trajectory
672 graph. We noticed that while the original trajectory graph generated by monocle3 corresponded
673 to the major cell lineages, it failed to connect some nodes that passed through populations of
674 cells expressing shared lineage markers. Moreover, some trajectory branches did not correspond
675 to biologically interpretable lineage progression, specifically the branches connecting two mature
676 neuronal cell types containing only adult cells. We corrected these issues by modifying the
677 trajectory according to the following principles: 1) if two terminal nodes failed to be connected
678 but were passing through populations of cells expressing known lineage-specific markers (such
679 as *RORB* for layer 4, *TLE4*/*SEMA4A* for layer 6b, *CUX2* for layer 2-3 and *CUX1* for layer 5-6-IT), we
680 connected these nodes 2) if a branch connected nodes located in two mature cell types, we
681 omitted this branch and 3) based on the first two principles, we isolated the shortest path
682 between the node in the neural progenitor/radial glia cluster and the node in the mature cell
683 type cluster.

684 **Identification of lineage-specific dynamically expressed genes**

First, we selected trajectory branches corresponding to specific lineages, as well as the cells along the branches. For the interneuron trajectory analysis, we only selected MGE or CGE cells from the GE progenitors cluster to analyze MGE and CGE-derived INs, respectively. Then, monocle3's Moran's test (graph_test function) was used to identify genes that are dynamically expressed in each lineage. We modified graph_test function to utilize Moran's test with covariates to ensure that our results are not affected by uneven contribution of cells from male and female subjects, different brain regions, as well as cells postmortem interval and 10x chemistry. We selected genes with adjusted p value < 0.05 as statistically significant dynamically expressed genes. To identify lineage-specific genes, we first compressed the single-cell expression data along each lineage by using a sliding window along pseudotime and averaging expression of neighboring cells for each gene. We generated 500 meta-cells in each lineage using this approach. Then, we fit the expression of each gene using a generalized linear model and the following formula: expression ~ splines::ns(pseudotime, df=3). Then, we calculated the area under the curve for the smoothed expression/pseudotime plot for each gene in each lineage across intervals of the sliding window. The difference of under the curve between the lineage of interest and all other lineages was used to rank genes according to their lineage specificity. Moran's p value < 0.05 and an expression difference of at least 20% in one section of the sliding window was used to define lineage-specific genes.

Analysis of single-cell ATAC-seq data and snRNA-seq/scATAC-seq integration

Four scATAC-seq datasets were first remapped to the same hg38 genome reference. Then, a minimal non-overlapping consensus peak set was created based on the peaks from all datasets, and ATAC-seq counts were mapped on this set of peaks using Signac (*34*), and the datasets were combined. Then, gene activity matrix for the combined dataset was generated by counting ATAC peaks in the promoter region and the gene body, using the same parameters as used by the Signac package. For mapping scATAC-seq data on the snRNA-seq dataset, we first integrated the two modalities using Seurat's FindTransferAnchors and the canonical correlation analysis (cca). We used the expression and gene activity of genes variable in the snRNA-seq datasets to perform cca and then used the TransferData function to map the scATAC-seq data on the snRNA-seq space followed by Harmony processing to regress the effect of different scATAC-seq and snRNA-seq chemistries. To map scATAC-seq profiles to the UMAP space and clusters we generated using snRNA-seq data, we identified 100 nearest neighbors for each scATAC-seq cell in the combined snRNA-seq/scATAC-seq space and then calculated the UMAP coordinates and cluster membership in the snRNA-seq space. To validate the accuracy of this procedure, we checked for the specificity of gene activity of cell type markers, as well as for age distribution. This integration and mapping procedure was repeated for the three major lineage classes (excitatory neurons, interneurons and macroglial cells).

SCENIC+ analysis

SCENIC+ requires single-cell transcriptomic and scATAC-seq data mapped to the same category (e.g. cluster) and also recommends generating pseudobulk scATAC-seq profiles prior to the analysis. In order to prepare our data for SCENIC+ analysis, we first selected ATAC-seq cells along the lineage trajectories using a sliding window approach and keeping the cells in cell type-specific clusters. Then, we generated 2500 meta-cell pseudobulk ATAC-seq profiles using the sliding

727 window along each trajectory and summing all ATAC counts. We also generated 2500 meta-cells
728 for the corresponding lineage-specific snRNA-seq profiles and restricted the analysis to lineage
729 and branch-specific genes relevant to each lineage. In order to generate pseudo-multiome
730 profiles from separate snRNA-seq and scATAC-seq datasets, we sorted cells into 10 bins based
731 on the pseudotime progression. These pseudotime bins were also used to identify differentially
732 accessible regions of chromatin and cis-regulatory topics using cisTopic (*35*), which was used with
733 default settings, except for setting the differential features threshold to 25%. After generating
734 pseudo-multiome profiles, we performed SCENIC+ analysis as described in the tutorial.
735 Significant enhancer-transcription factor-gene relationships in each lineage were exported as the
736 final result.

737 **Identification of sex and region-enriched dynamically expressed genes**

738 To identify male and female-enriched genes in each lineage, we selected cells from only males or
739 females within each lineage and first performed Moran's I test separately for male and female
740 data. Then, we compressed the data and calculated area under the curve for male and female
741 gene expression. Genes with Moran's I statistic >= 0.1, adjusted Moran's p value<0.05 and the
742 area under curve difference between male and female expression >= 50 were considered sex-
743 specific in each given lineage.

744 **Gene ontology analysis**

745 We used ShinyGO (*36*) to perform gene ontology analysis using genes expressed in each lineage
746 as the background gene list. In order to reduce redundancy of the identified GO terms, all
747 significant (adjusted p value < 0.05) terms were used as input to Revigo (*37*) in case more than
748 10 pathways were identified. The value of the resulting gene list of 0.4 was used. The -log10(p
749 value) and fold enrichment for the resulting non-redundant GO processes were reported.

750 **Analysis of enrichment of disease risk genes**

751 We intersected disease risk gene lists with our list of lineage-specific genes, as well as genes
752 enriched in male and female developmental lineages. We calculated hypergeometric p values for
753 each overlap, using genes expressed in each lineage as the background.

754 **Data visualization**

755 Cell type, gene expression and lineage trajectories for each lineage can be visualized at
756 https://pre-postnatal-cortex.cells.ucsc.edu.

757 **MERSCOPE spatial transcriptomics**

758 Sample preparation was performed according to manufacturer's instructions (MERSCOPE Fresh
759 and Fixed Frozen Tissue Sample Preparation User Guide, Doc. number 91600002). Briefly, fresh
760 snap frozen tissue with a high RNA integrity number (RIN>8) were sectioned (10um thick) using
761 a cryostat and mounted on MERSCOPE functional slides. Sections where then fixed and stored at
762 70% ethanol for up to two weeks. Sections went through autofluorescence quenching under UV
763 light for 3 hours using the MERSCOPE Photo-bleacher instrument. A Pre-designed panel mix (140
764 genes) focused on early emerging excitatory lineage-specific genes based on the single-nuclei
765 analysis were used for probe hybridization. Hybridizations were performed at 37°C for up to 48
766 hours in a humid environment. Post prob hybridization, sections were fixed using formamide and

767 embedded in gel. After gel embedding, tissue samples were cleared using a clearing mix solution
768 supplemented with proteinase K for 24-48 hours at 37°C until no visible tissue was evident in the
769 gel. After clearing was completed, sections were stained for DAPI and PolyT and fixed with
770 formamide prior to imaging. No additional cell boundary stainings were used. The MERSOPE
771 imaging process was done according to the MERSCOPE Instrument Site Preparation Guide (Doc.
772 Number 91500001). Briefly, an imaging kit was thawed at 37°C for 45 minutes, activated and
773 loaded into the MERSCOPE instrument. The flow chamber was then assembled, fluidics were
774 primed, flow chamber filled with liquid and a low-resolution image was taken. Based on DAPI
775 staining, an ROI was chosen for the full imaging experiment. After imaging was complete, data
776 was processed using MERSCOPE proprietary software. Further analysis, visualization, and
777 integration of spatial data, was done using Seurat v5 (Source: vignettes/spatial_vignette_2.Rmd).
778 Putative neuronal layer localization was predicted from co-localization with referenced markers
779 at relevant developmental stages.

780

781

782

783

Table S1. Sample and nuclei metadata.

Table S2. Lineage and branch-specific genes.

Table S3. Results of eGRN analysis using SCENIC+.

Table S4. Results of region-specific gene expression analysis.

Table S5. Sex-enriched developmentally regulated genes.

Table S6. Lineage- and sex-specific disease risk genes.

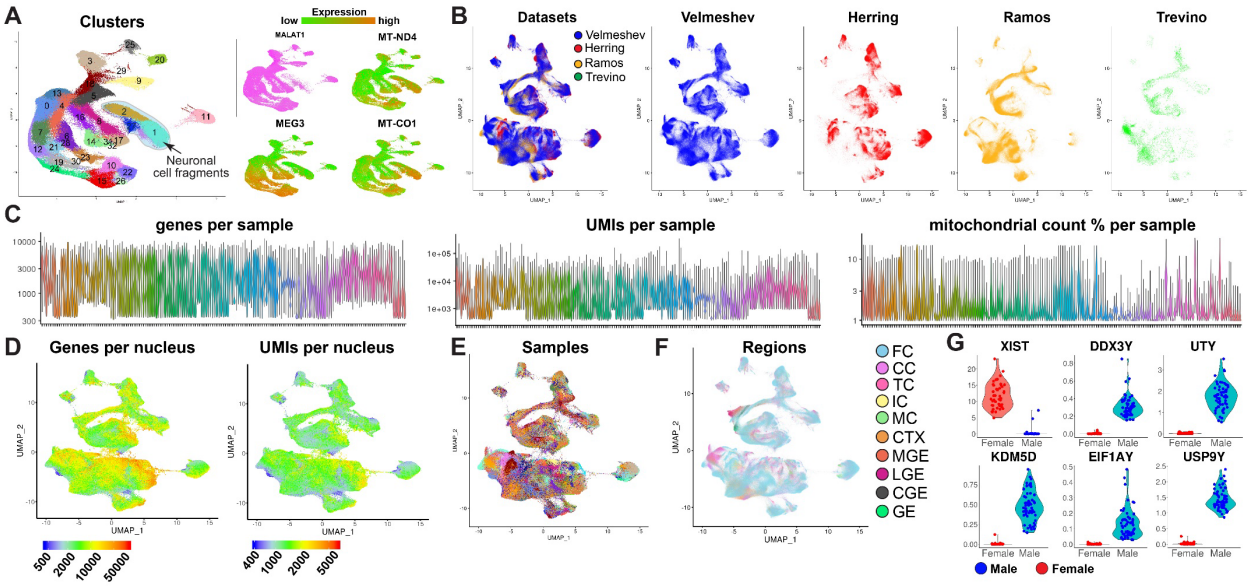

Figure S1. Technical and biological characteristics of the combined snRNA-seq dataset. A) Identification of the clusters containing neuronal debris. **B)** Integration of the current dataset with previously published datasets. **C)** Gene and UMI counts per nucleus, as well as mitochondrial reads ratio across all samples. **D)** Gene and UMI counts per nucleus across all cell types. **E-F)** Distribution of nuclei from different samples and regions. FC-frontal/prefrontal cortex, CC-cingulate cortex, TC-temporal cortex, IC-insular cortex, MC-motor cortex, CTX-cortex. **G)** Expression of sex-specific genes used to determine sex of samples with unknown status.

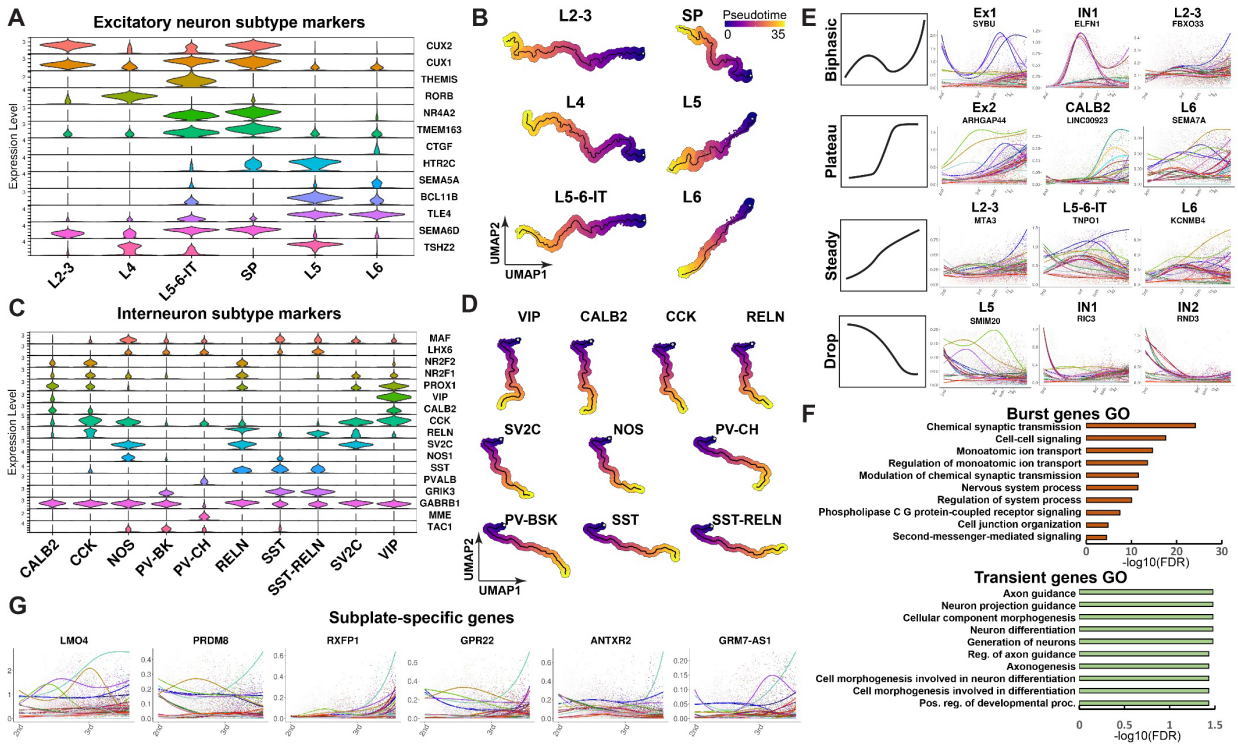

Figure S2. Excitatory neuron and interneuron lineage analysis. A) Expression of cortical excitatory neuron marker genes used to determine excitatory neuron lineages. **B)** Isolated lineages trajectories for excitatory neuron subtypes. **C)** Markers of interneuron subtypes. **D)** Isolated interneuron trajectories. **E)** Examples of biphasic, plateau, steady and drop expression of lineage and branch-specific genes. **F)** GO pathways enriched for burst and transient neuronal genes. **G)** Top subplate-specific dynamically expressed genes.

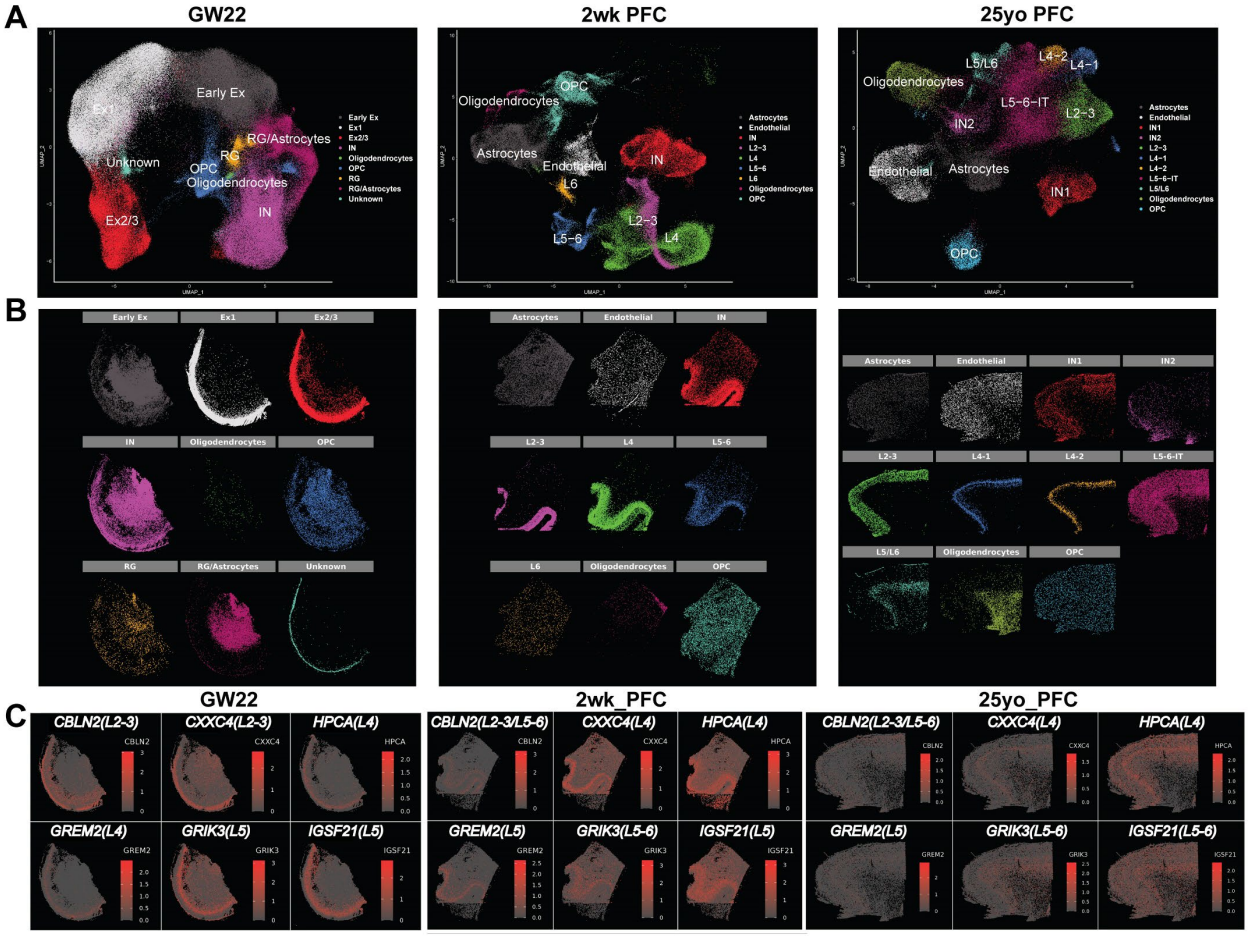

Figure S3. Spatial transcriptomic analysis of lineage-specific genes across development. A) UMAP embedding of annotated clusters. **B)** Spatial localization patterns of individual clusters (cluster colors and spatial location correspond with Fig. 2g). **C)** Spatiotemporal expression of layer-specific markers.

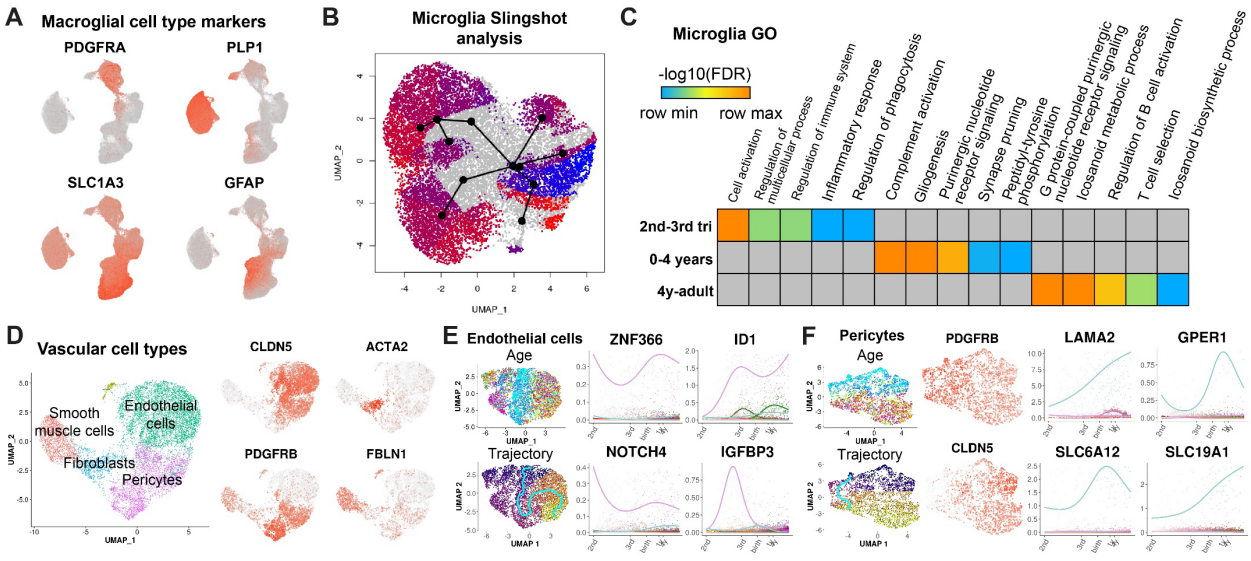

Figure S4. Analysis of glial and vascular lineages. A) Markers of OPCs, oligodendrocytes, fibrous and protoplasmic astrocytes **B)** Slingshot analysis of microglial lineage trajectories. **C)** Gene ontology analysis developmental microglia genes. **D)** Analysis of vascular cell types. **E-F)** Trajectory analysis of endothelial cells and pericytes.

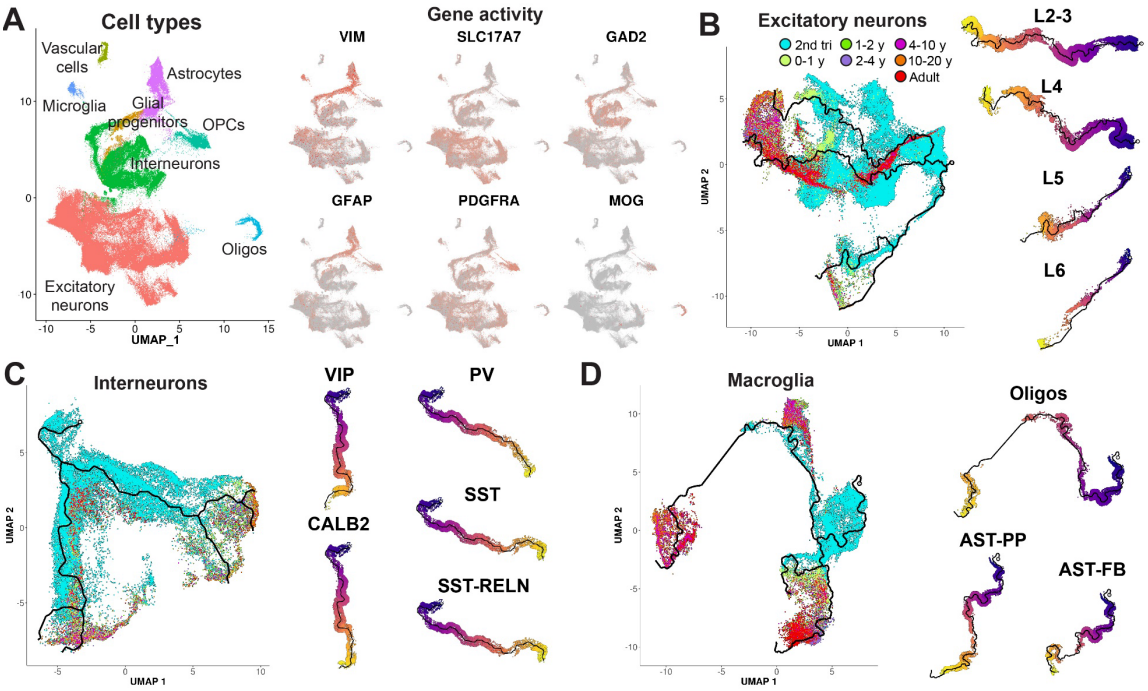

Figure S5. Mapping developmental scATAC-seq to specific lineage trajectories. A) Gene activities of cell type-specific marker genes. **B-D)** Age distribution and selection of ATAC-seq cells for specific lineages of excitatory neurons **(B)**, interneurons **(C)** and macroglial cells **(D)**.

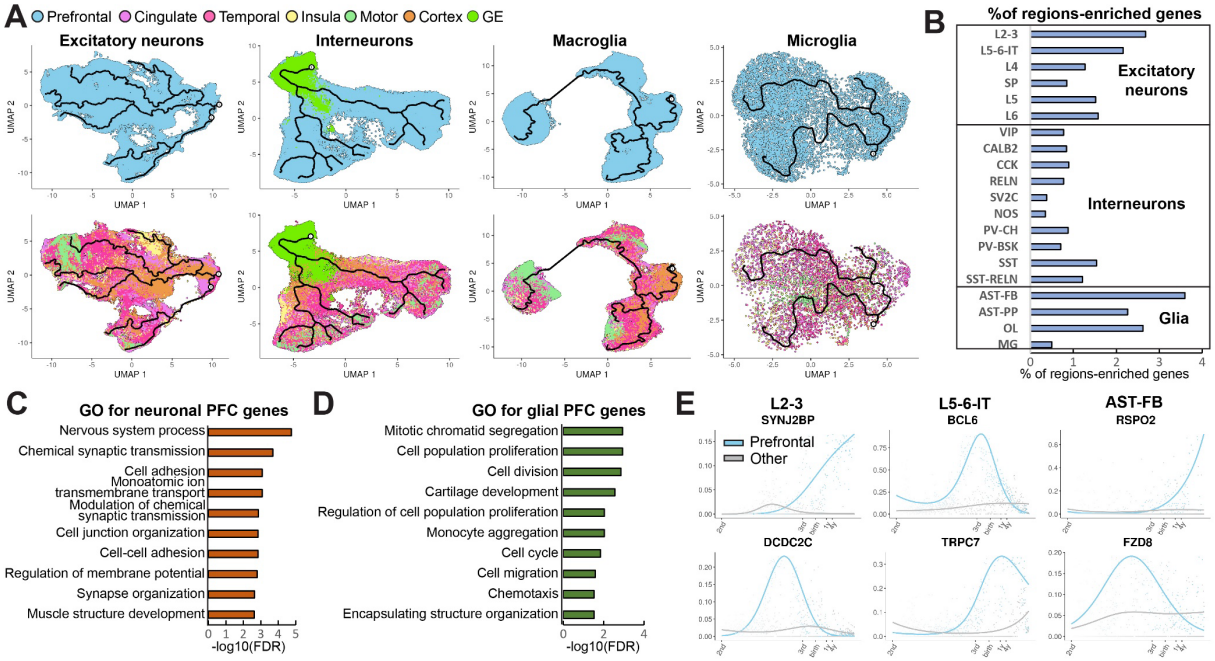

Figure S6. Frontal cortex-specific developmental programs. A) Cells from the frontal/prefrontal cortex and other cortical regions in the excitatory neuron, interneuron, macroglial and microglial lineages. **B)** Number of PFC-specific genes in neuronal and glial lineages relative to the total number of genes expressed in each lineage. **C-D)** Gene ontology analysis of PFC-specific genes in neuronal and glial lineages. **E)** Examples of top genes enriched in the PFC in specific lineages.

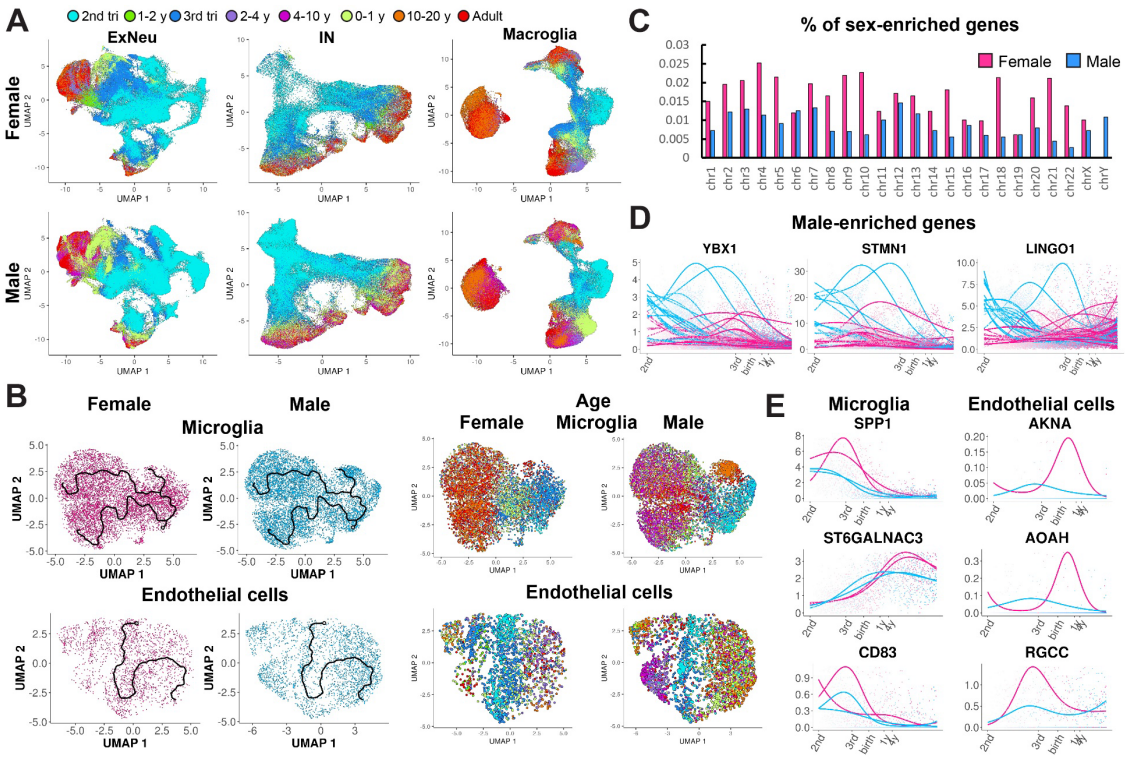

Figure S7. Analysis of sex and region-enriched genes during microglia and endothelial cell development. A) Female and male microglia and endothelial cell trajectories. **B)** relative number of sex-specific genes per chromosome. **C)** Examples of top male-enriched genes. **D)** Female and male trajectories in microglia and endothelial cells. **E)** Top female-enriched genes expressed in microglia and endothelial cells.

References

31. I. Korsunsky *et al.*, Fast, sensitive and accurate integration of single-cell data with Harmony. *Nature Methods* **16**, 1289-1296 (2019).
32. E. Z. Macosko *et al.*, Highly Parallel Genome-wide Expression Profiling of Individual Cells Using Nanoliter Droplets. *Cell* **161**, 1202-1214 (2015).
33. X. Qiu *et al.*, Reversed graph embedding resolves complex single-cell trajectories. *Nature Methods* **14**, 979 (2017).
34. T. Stuart, A. Srivastava, S. Madad, C. A. Lareau, R. Satija, Single-cell chromatin state analysis with Signac. *Nature Methods* **18**, 1333-1341 (2021).
35. C. Bravo González-Blas *et al.*, cisTopic: cis-regulatory topic modeling on single-cell ATAC-seq data. *Nature Methods* **16**, 397-400 (2019).
36. S. X. Ge, D. Jung, R. Yao, ShinyGO: a graphical gene-set enrichment tool for animals and plants. *Bioinformatics* **36**, 2628-2629 (2019).
37. F. Supek, M. Bošnjak, N. Škunca, T. Šmuc, REVIGO summarizes and visualizes long lists of gene ontology terms. *PLoS One* **6**, e21800 (2011).